# Subband structure and band bending in symmetric modulation-doped double quantum wells

F. Ungan<sup>1</sup>, E. Ozturk<sup>1,a</sup>, Y. Ergun<sup>1</sup>, and I. Sokmen<sup>2</sup>

Received: 30 October 2003 / Received in final form: 30 January 2004 / Accepted: 1st July 2004 Published online: 21 December 2004 – © EDP Sciences

**Abstract.** We have calculated the subband structure and confinement potential of modulation-doped  $Ga_{1-x}Al_xAs$ -GaAs symmetric double quantum wells a function of the doping concentration. Electronic properties of this structure are determined by solving the Schrödinger and Poisson equations self-consistently. To understand the exchange correlation potential effects on the band bending and subband populations, this potential has been included in the calculation at 0 K and, at room temperature. We find that at low doping concentrations the effect of the exchange correlation potential is more pronounced on the subband populations.

**PACS.** 73.90.+f Other topics in electronic structure and electrical properties of surfaces, interfaces, thin films, and low-dimensional structures

## 1 Introduction

There has recently, been interest in the electronic properties of double-quantum well structures (DQW), because they are expected to form the basis for applications in novel electronic devices [1–10]. In many of the theoretical calculations, the electron gas (EG) systems within the quantum wells have been treated as two-dimensional (2D). Two dimensional electron gas (2DEG) systems confined in semiconductor space charge layers have provided an ideal laboratory for studying many-body exchange-correlation effects in electron-electron interactions. The symmetric coupled DQWs deserve closer attention owing to their attractive physical properties and promising technical applications. In DQW structures, interlayer correlations play a fundamental role in the many-body behaviour of the electronic system [11]. Many-body effects arising from exchange-correlation corrections due to the presence of free carriers in the system manifest themselves also in the renormalization of 2D subband energies, when there is a finite occupation with electrons of the corresponding states [12]. The correlation effects in DQWs have also been studied [13–15].

In this paper, for symmetric DQWs we have theoretically investigated the exchange-correlation effects as dependent on the doping concentration, at 0 K and 300 K. We have seen that the exchange-correlation effect changes the potential profile and the subband populations as de-

pendent on the doping concentration and temperature, and this change is more pronounced at low donor concentration. In addition, we have found that the total thickness  $(L_D)$  of symmetric DQWs is very sensitive to the donor concentration. We will examine the influence of an applied electric field on symmetric and asymmetric DQWs, in a future publication.

# 2 Theory

The electronic structure of a DQW has been solved using a self-consistent calculation under the effective-mass approximation. We have calculated the confining potential, the charge density, the subband energies and the subband populations self-consistently by solving the Schrödinger and Poisson equations.

Figure 1 shows the schematic illustration for a symmetric DQW structure. The origin for z is taken to be the centre of the structure.  $Ld_1$  and  $Ld_2$  are the doped  $\mathrm{Al}_x\mathrm{Ga}_{1-x}\mathrm{As}$  thicknesses,  $Ls_1$  and  $Ls_2$  are the undoped  $\mathrm{Al}_x\mathrm{Ga}_{1-x}\mathrm{As}$  thicknesses,  $Lw_1$  and  $Lw_2$  are the GaAs quantum well thicknesses, and Lb is the  $\mathrm{Al}_x\mathrm{Ga}_{1-x}\mathrm{As}$  barrier thickness.

The single-electron one-dimensional Schrödinger equation can be written as

$$\left(-\frac{\hbar^2}{2m^*}\frac{d^2}{dz^2}+V(z)\right)\psi_{\scriptscriptstyle i}(z)=E_{\scriptscriptstyle i}\psi_{\scriptscriptstyle i}(z) \eqno(1)$$

<sup>&</sup>lt;sup>1</sup> Cumhuriyet University, Department of Physics, 58140 Sivas, Turkey

<sup>&</sup>lt;sup>2</sup> Dokuz Eylul University, Department of Physics, Izmir, Turkey

 $<sup>^{\</sup>rm a}$  e-mail: eozturk@cumhuriyet.edu.tr

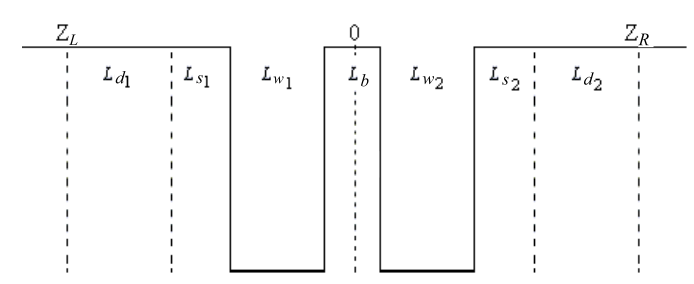


**Fig. 1.** Schematic illustration for a symmetric DQW structure based on GaAs-  $Al_xGa_{1-x}As$  materials.  $Ld_1$  and  $Ld_2$  are the doped  $Al_xGa_{1-x}As$  thicknesses,  $Ls_1$  and  $Ls_2$  are the undoped  $Al_xGa_{1-x}As$  thicknesses,  $Lw_1$  and  $Lw_2$  are the GaAs quantum well thicknesses, Lb is the  $Al_xGa_{1-x}As$  barrier thickness, and  $L_D = Z_L + Z_R$  is the total thickness of DQW.

where  $m^*$  is the electron effective mass,  $V(z) = V_H(z) + V_{xc}(z)$  is an effective potential,  $V_H(z)$  is the Hartree potential and  $V_{xc}(z)$  is the exchange-correlation potential. The Hartree potential  $V_H(z)$  is determined by the Poisson equation

$$\frac{d^2V_H(z)}{dz^2} = -\frac{4\pi e^2}{\varepsilon} [N(z) - N_d(z)] \tag{2}$$

where  $\varepsilon$  is the GaAs dielectric constant and  $N_d(z)$  is the total density of ionized dopants. The electron density is related to the electronic wave functions by the relation

$$N(z) = \sum_{i=1}^{n_d} n_i |\psi_i(z)|^2$$
 (3)

where  $n_d$  is the number of filled states,  $n_i$  is the temperature-dependent number of electrons per unit area in the ith subband given by

$$n_i = \frac{m^* k_B T}{\pi \hbar^2} \ln\{1 + \exp[(E_F - E_i)/k_B T]\}$$
 (4a)

and at zero temperature

$$n_i = \frac{m^*}{\pi \hbar^2} (E_F - E_i) \tag{4b}$$

where i is a subband index,  $k_B$  is the Boltzmann constant and  $E_F$  represents the Fermi energy. According to reference [16], at the low-temperature limit  $(T \to 0)$ , the Fermi energy can be taken as the donor level, which is supposed to lie at an energy Ed = 0.070 eV below the conduction band of the GaAs layers. All donors are assumed to be ionized i.e.

$$Ld_1 \times Nd_1 + Ld_2 \times Nd_2 = \sum_{i=1}^{n_d} n_i$$
 (5)

where  $Nd_1$  is the doping concentration for  $Ld_1$  thickness and  $Nd_2$  is the doping concentration for  $Ld_2$  thickness.

For the exchange-correlation potential, we use the parameterized analytic expression under the local-density

approximation [17]

$$V_{xc} = -0.985 \frac{e^2}{4\pi\varepsilon_0\varepsilon_r} n^{1/3} (z)$$

$$\times \left\{ 1 + \frac{0.034}{a_b^* n^{1/3} (z)} \ln \left[ 1 + 18.376 a_b^* n^{1/3} (z) \right] \right\}$$
(6)
$$a_b^* = 4\pi\varepsilon_0\varepsilon_r \hbar^2 / m_0^* e^2.$$

The self-consistent solution of (1)–(6) gives the potential profile, the density profile, the subband energies and the subband populations.

#### 3 Results and discussions

We have investigated theoretically the electronic structure of  $GaAs-Al_xGa_{1-x}As$  DQW for different doping concentrations, as dependent on exchange-correlation effects and temperature. We assume that these layers are symmetric with respect to the origin, i.e. they have the same thickness  $(Ls_1 = Ls_2 = 10 \text{ Å}, Ld_1 = Ld_2, Lw_1 = Lw_2 = 100 \text{ Å})$ and the same doping concentration  $(Nd_1 = Nd_2)$ . Figure 2 shows the confining potential and the subband energies with their squared wave functions with  $Nd_1 = 5 \times$  $10^{17} \,\mathrm{cm}^{-3}$ ,  $Lb = 25 \,\mathrm{\mathring{A}}$ ,  $Ed = E_F = 70 \,\mathrm{meV}$ , x = 0.33, (x is the aluminium content in the  $Al_xGa_{1-x}As$  layers), at T =0 K. The dashed curves include exchange-correlation (xc) effects and the solid curves neglect exchange-correlation (nxc) interaction. As seen from this figure the subband energy levels appear as doublets because of tunnelling between the two wells, and the structure is slightly changed with the introduction of exchange-correlation effects.

For T=0 K and T=300 K, Figures 3a, b show the xc and nxc potential profiles for two doping concentrations. In the self-consistent calculation, we assume that Fermi energy is constant at T=0 K (i.e.  $E_F=Ed$ ) and is variable at T=300 K. In this figure, the Fermi energy is set to 0 eV. As seen from Figure 3, the xc effect is more pronounced at low doping concentration  $(Nd_1=1\times10^{17}~{\rm cm}^{-3})$ , at T=0 K. This effect is less pronounced at T=300 K.

For different doping concentrations  $(Nd=(1,\,5,\,10)\times 10^{17}~{\rm cm}^{-3})$  the electronic density profiles which include the xc and nxc potential are displayed in Figure 4. At high donor concentrations, an increasing charge density in the confining potential leads to more band bending and gives rise to the formation of a deeper quantum well (see Fig. 3a). While for  $Nd=1\times 10^{17}~{\rm cm}^{-3}$  the density profile is localized at the centre of the quantum wells, for  $Nd=5\times 10^{17}~{\rm cm}^{-3}$  the density profile is more localized at the deep regions of the quantum wells and gives a new little peak near the barrier. This new density peak increases with the donor concentration. We have seen that the exchange-correlation potential effect is less pronounced at high donor concentration. These features could be of use in controlling the confinement of carriers in semiconductor devices.

The subband populations versus the doping concentration are represented in Figures 5a, b at  $T=0~\mathrm{K}$ 

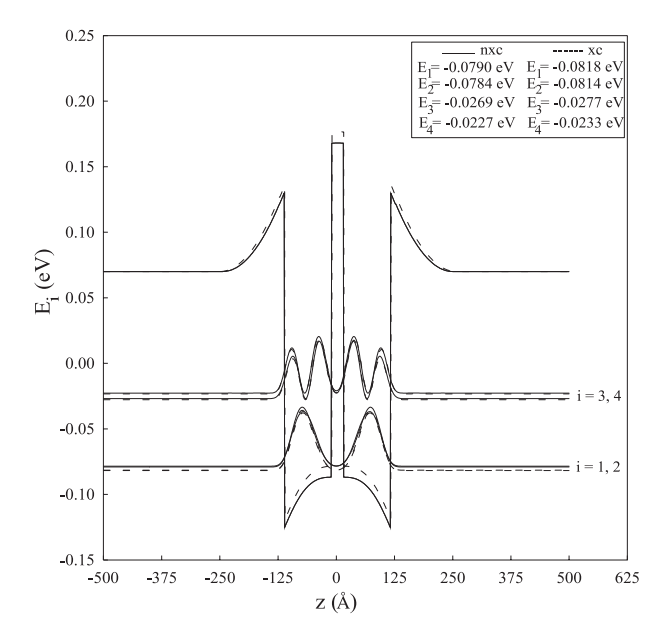
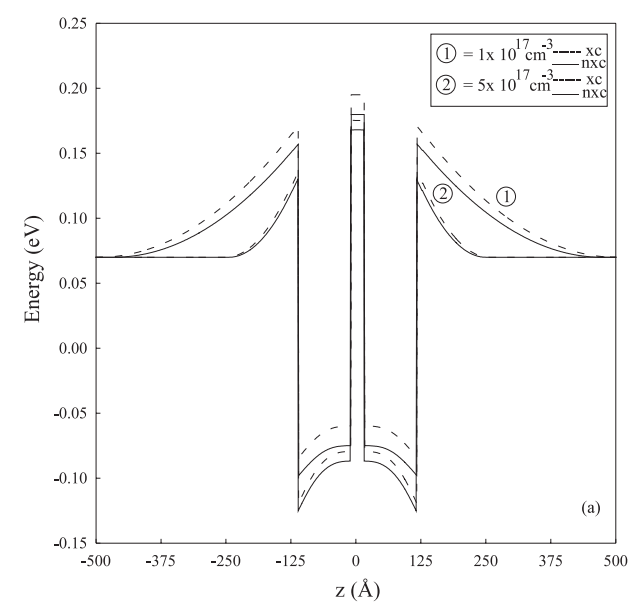
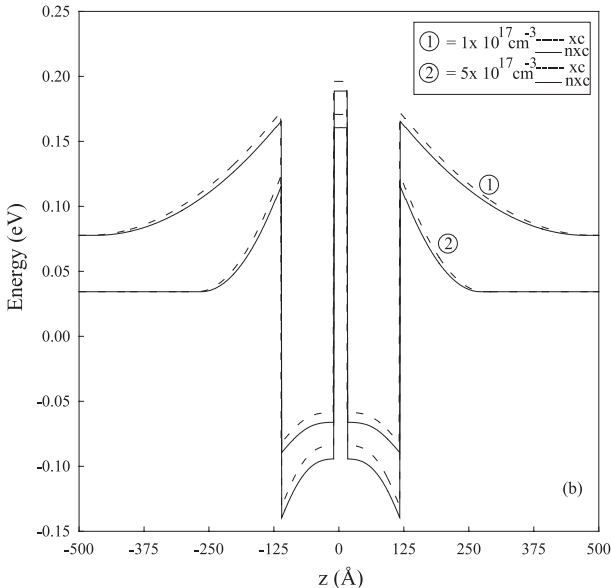


Fig. 2. The confined potential and the subband energies with their squared wave functions with  $Nd = 5 \times 10^{17}$  cm<sup>-3</sup>, at T = 0 K. The Fermi energy is set at 0 eV. The dashed curves show exchange-correlation (xc) effect and the solid curves represent non-exchange-correlation (nxc) effect.

and T = 300 K, respectively. The solid curves represent nxc effects; the dashed curves represent xc interactions. As expected the subband populations and the number of filled states increase with donor concentration. The change in the subband occupation depends on the doping concentration, the exchange-correlation interaction and temperature. As seen from these figures, at low doping concentrations the subband populations change with the exchange-correlation effect, but these changes are smaller at high donor concentrations [18]. As can be seen from equation (4a) the subband population increases slightly with increasing temperature owing to both the exponential term in the logarithm and the linear prefactor term. Temperature has a certain effect on the shape of the confining potential because of thermal excitation of the electrons from the lowest subband into these higher ones.

Figure 6 shows the difference between the first subband populations with exchange-correlation (xc) and nonexchange-correlation (nxc) over the doping concentration  $(\Delta n/Nd)$  as a function of the doping concentration. The solid curve is for T = 0 K and the dashed curve is for T = 300 K. As seen from this figure, this proportion is much greater at room temperature for low doping concentration. By increasing the doping concentration, the proportions approach each other. We have said that this proportion is not effective on the subband populations at high doping concentration. Thus, the donor concentration can be used as the fitting parameter in these systems. We have seen that at room temperature, the carriers which appear because of the impurity atoms are more efficient than the exchange-correlation effect and temperature on the subband population.

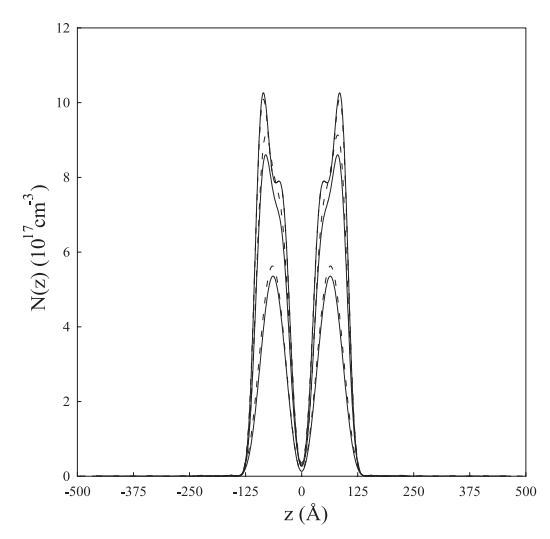




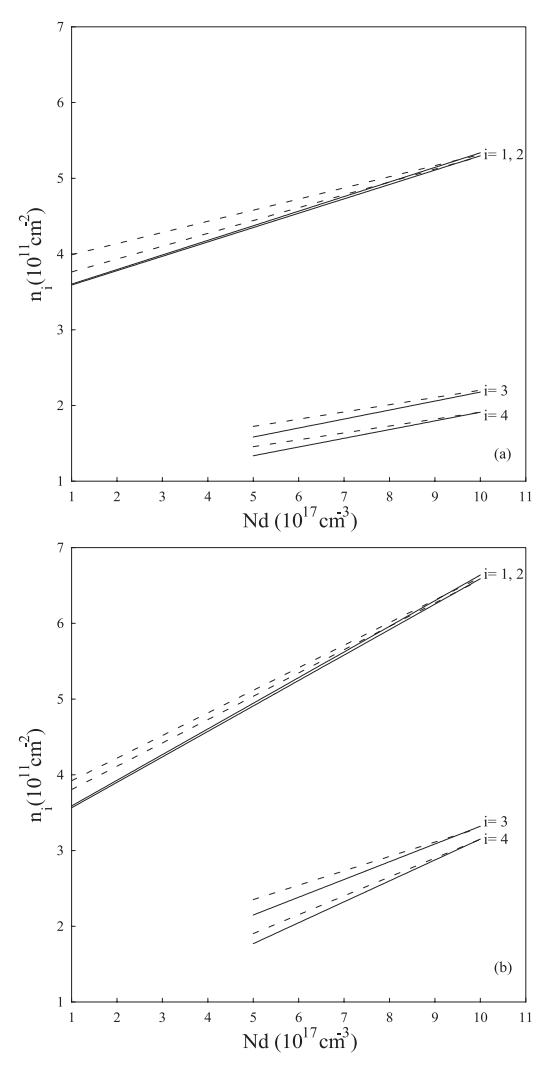
**Fig. 3.** For two doping concentrations the xc and nxc potential profiles at (a) T=0 K and (b) T=300 K. Fermi energies are set at 0 eV.

Figure 7 shows the total thickness  $(L_D)$  of GaAs-Al<sub>x</sub>Ga<sub>1-x</sub>As symmetric DQW versus the doping concentration. While the solid curves represent nxc effects, the dashed curves represent xc effects. We have used an iteration method to solve the Schrödinger and Poisson equations self-consistently. In the calculations, the depletion lengths  $(Ld_1 = Ld_2)$  in the doped Al<sub>x</sub>Ga<sub>1-x</sub>As layers are used as input parameters, because the convergence is satisfied for a given doping concentration. The total thickness  $(L_D)$  of DQW changes depending on the doping concentration. From the self-consistent calculation, we have shown that the total thickness and the xc effect decreases with the doping concentration.

In conclusion, we have investigated the electronic structure of  $GaAs-Al_xGa_{1-x}As$  symmetric DQWs. To



**Fig. 4.** The electronic density profiles with (dotted line) xc and (solid line) nxc effect for different doping concentrations (from bottom to top)  $Nd_1 = (1, 5, 10) \times 10^{17} \text{ cm}^{-3}$ , at T = 0 K.



**Fig. 5.** The subband populations as a function of the doping concentration at (a) T=0 K and (b) T=300 K. The dashed curves represent the xc effect and the solid curves represent the nxc effect.

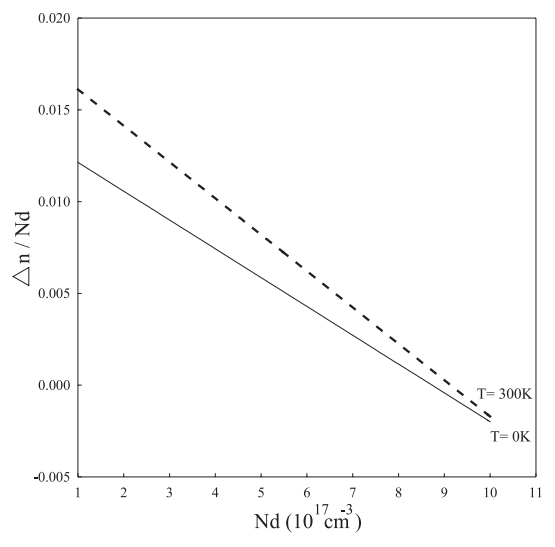


**Fig. 6.** The difference between the ground subband population with xc and nxc effect  $(\Delta n = n_{xc} - n_{nxc})$  over the doping concentrations versus the doping concentration. The dashed curve is for T = 300 K and the solid curve is for T = 0 K.

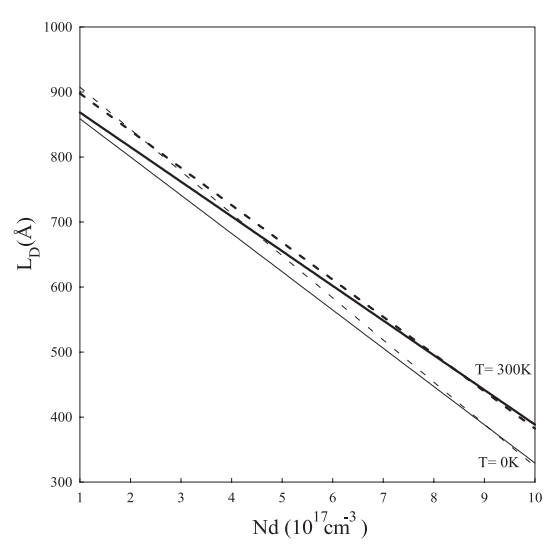


Fig. 7. The change of total thickness  $(L_D)$  of the symmetric DQW versus doping concentration. The thick dashed curve is for the xc effect at T=300 K and the thick solid curve is for the nxc effect, at T=300 K. The thin dashed curve represents the xc effect at T=0 K and the thin solid curve represents the nxc effect at T=0 K.

determine the subband structure, the self-consistent methods of the Schrödinger and Poisson equations were used. We have studied the effect of the exchange-correlation interactions and temperature on the doping concentration. From our calculations, we have seen that the high doping concentration leads to strong confining effects, thus the donor concentration Nd can be used as a tuneable parameter of these semiconductor devices. In addition it was seen that the change in subband properties due to exchange-correlations effects and temperature is more pronounced at low doping concentration. The total thickness of symmetric DQW is very sensitive to the doping concentration.

The authors would like to thank the Prime Ministry State Planning Organization in Turkey (DPT) grand No. DPT-2001.K.120330 for financial support.

## References

- R. Decca, A. Pinczuk, S. Das Sarma, L.N. Pfeiffer, K.W. West, Phys. Rev. Lett. 72, 1506 (1994)
- 2. C. Zhang, Phys. Rev. B 49, 2939 (1994)
- P.I. Tamborenea, S. Das Sarma, Phys. Rev. Lett. 73, 1971 (1994)
- J.P. Eisenstein, L.N. Pfeiffer, K.W. West, Phys. Rev. Lett. 69, 3804 (1992)
- P. Johansson, J.M. Kinaret, Phys. Rev. L 71, 1435 (1993)
- Y. Hatsugai, P.A. Bares, X.G. Wen, Phys. Rev. Lett. 71, 424 (1993)
- Y. Ohno, T. Matsusue, H. Sakaki, Appl. Phys. Lett. 62, 1952 (1993)
- 8. K. Leo, J. Shah, E. Göbel, J.P. Gordon, S. Schmitt-Rink, Semicond. Sci. Technol. 7, B394 (1992)

- N. Tsukada, A.D. Wieck, K. Ploog, Appl. Phys. Lett. 56, 2547 (1990)
- Xin-Hai Liu, Xue-Hua Wang, Be-Yuan Gu, Phys. Rev. B 64, 195322 (2001)
- D.S. Kainth, D. Richards, H.P. Hughes, M.Y. Simmons,
   D.A. Ritchie, Phys. Rev. B 59, R2065 (1998);
   D.S. Kainth,
   D. Richards, A.S. Bhatti, H.P. Hughes, M.Y. Simmons,
   E.H. Linfield, D.A. Ritchie, Phys. Rev. B 59, 2095 (1999)
- D.A. Kleinman, R.C. Miller, Phys. Rev. B 32, 2266 (1985);
   S. Das Sarma, R. Jalabert, S.-R.E. Yang, Phys. Rev. B 41, 8288 (1990)
- S. He, S. Das Sarma, X.C. Xie, Phys. Rev. B 47, 7312 (1993)
- 14. G. Boebinger et al., Phys. Rev. Lett. 64, 1793 (1990)
- H.A. Fertig, Phys. Rev. B **40**, 1087 (1989); A.H. Macdonald, P.M. Platzman, G.S. Boebinger, Phys. Rev. Lett. **65**, 775 (1990); L. Brey, Phys. Rev. Lett. **65**, 903 (1990); X. Chen, J.J. Quinn, Phys. Rev. Lett. **67**, 895 (1991); S. He et al., Phys. Rev. B **43**, 9339 (1991)
- 16. L. Hedin, B.I. Lundqvist, J. Phys. C 4, 2064 (1971)
- 17. W. Xu, Int. J. Mod. Phys. B 10, 1293 (1996)
- 18. M.H. Degani, Phys. Rev. B 44, 5580 (1991)